Postprint of: Malikan, M., Temperature influences on shear stability of a nanosize plate with piezoelectricity effect, Multidiscipline Modeling in Materials and Structures, Vol. 14, No. 1 (2018), pp. 125-142.
https://doi.org/10.1108/MMMS-09-2017-0105

Temperature influences on shear stability of a nanosize plate with piezoelectricity effect

Mohammad Malikan
Department of Mechanical Engineering, Islamic Azad University, Mashhad Branch, Mashhad, Iran
Call: mohammad.malikan@yahoo.com, +98 938 778 0652,

Abstract

The present work aims to show thermal environment effects on shear buckling of a piezoelectric nanoplate using modified couple stress theory with various boundary conditions. A piezoelectric nanoplate is embedded in thermal environment and an external electric voltage is applied on the plate. A simplified first order shear deformation theory has been employed and governing differential equations have been obtained using Hamilton's principle and nonlinear strains of von Kármán. Modified couple stress theory has been applied to considering nanoscale effects. An analytical approach was applying to obtain Results with various boundary conditions. Subsequently, results have been presented by change in some parameters, such as; aspect ratio, effect of various boundary conditions, effect of thermal environment, electric voltage and length scale parameter influences. Results showed that the impact of external electric voltage on the critical shear load is more than thermal environment effects.

Keywords: Piezoelectric nanoplate; Modified couple stress theory; Simplified first order shear deformation theory

1. Introduction

Due to the peculiar properties, piezoelectric materials have found extremely wide applications in the fields of electrical, ultrasonic, robotics, energy conversion, medicine, space, domestic industries and many others [1]. Piezoelectric materials, with their ability to generate electrical charges when subjected to a mechanical pressure, are the materials of choice for all the applications in which electro-mechanical transduction is needed, and represent one of the most valuable class of materials in biomedical applications [2, 3]. Piezoelectric crystals are exploited either in direct piezoelectric effect – a mechanical stress applied to the crystal causes charge generation in the material or in the converse piezoelectric effect - electric field applied to the material generates a strain. Piezoelectricity basically depends on crystal lattice structure, and lack of a center of symmetry in the unit crystal cell is the necessary requirement for a material to show piezoelectricity in any form (pyroelectricity and ferroelectricity) [4]. Most important classes of piezoelectric materials are represented by ceramic perovskite materials [4], such as $BaTiO_3$, lead titanate (PT), lead zirconate titanate ceramics (PZT), lead lanthanum zirconate titanate (PLZT), and lead magnesium niobate (PMN).

Over the past two decades, many researches have been being examined in order to study the stability behavior of nano structures [5-41]. Malekzadeh et al. [8] considered the Small scale effect on the thermal buckling of orthotropic arbitrary straight-sided quadrilateral nanoplates embedded in an elastic medium via classical plate theory. Ke et al. investigated the nonlinear vibration [9] and post-buckling [10] behaviors of nonlocal Timoshenko piezoelectric nanobeams under combined thermo-electro-mechanical loadings. Murmu et al. [11] conducted buckling analysis of bi-layer nano graphene in nonlocal theory under biaxial compression via analytical solution using the classical plate theory with linear strains. It also demonstrated that nonlocal critical load was always less than local critical load. Malekzadeh and Alibeygi [12] analyzed the thermal buckling of orthotropic single layer graphene sheet using nonlinear elastic foundation. The classical theory and differential quadrature method were used together with the Winkler elastic foundation modeled with the nonlinear spring. Mohammadi et al. [13] studied the shear

buckling of orthotropic rectangular single layer nanoplates in thermal environment by classical plate theory. They showed that the difference between the shear buckling load calculated by isotropic and orthotropic plates decreases with increasing nonlocal parameter. Radic et al. [14] published a study on mechanical buckling of multi-layers rectangular graphene sheet based on an elastic foundation and found that the nonlocal effect has great influence on higher buckling modes. The analytical solution for vibrations and biaxial buckling of multilayers graphene sheet based on the Winkler elastic foundation were investigated by Murmu et al. [15]. The presented equations utilized classical plate theory and proved that the critical temperature and natural frequencies were further affected by reducing the Winkler coefficient in high modes. Anjomshoa et al. [16] derived mechanical buckling equations of multi-layers of rectangular graphene sheets placed on an elastic foundation using the classical plate theory and finite element numerical method. Radebe and Adali [17] studied the buckling of rectangular nanoplates with uncertain orthotropic material properties using a nonlocal theory. They considered nanoplate as a nonlocal plate to take the small-size effects into account with small-scale parameter also taken to be uncertain. They studied the effect of small scale on natural frequencies. Vibration and buckling analysis of a piezoelectric nanoplate considering surface effects and in-plane constraints have been presented by Jiang and Yan [18]. Golmakani and Rezatalab [19] conducted a study on the biaxial buckling of single layer graphene plate by considering the elastic foundation and nonuniform mechanical load. The results showed that by neglecting the elastic foundation, when the small scale effects are reduced, the critical load also has decreased. Challamel et al. [20] proposed the buckling and vibrations of micro structure rectangular plates considering phenomenological and lattice-based nonlocal continuum models. Radic and Jeremic [21] studied the thermal buckling of double-layered graphene sheets embedded in an elastic medium with various boundary conditions using a nonlocal new first-order shear deformation theory. Their results showed that in nonlinear distributions of temperature all over the thickness of plate, have a higher value of critical buckling temperatures for lower values of aspect ratio. Malikan et al. [22] published buckling of double-layered nanoplate under shear and thermal loads based on an elastic matrix using differential quadrature method. Fang and Zhu [23] presented size-dependent nonlinear vibration of nonhomogeneous shell embedded with a piezoelectric layer based on surface/interface theory. By applying nonlinear strains in Donnell shell theory and using Runge-Kutta method for solving simple boundary condition, the results showed that the vibration amplitude in the whole frequency region increases with increasing residual stress, elastic and piezoelectric constant of surface. Fang et al. [24] studied surface energy effect on nonlinear free vibration behavior of orthotropic piezoelectric cylindrical nano-shells. The governing equations of motion were solved by using the homotopy perturbation method (HPM). It was found that for a fixed thickness or dimensionless amplitude, the effect of surface elastic constant on the nonlinear free vibration behavior is similar to surface piezoelectric constant, but opposite to surface dielectric constant.

This paper investigates new theoretical considering on piezoelectric nanoplates under shear buckling in thermal environment. Regarding FSDT, we could not find the exact value for shear correction factor to considering the shear stress distribution in thickness direction. Therefore, the simplified first order shear deformation theory (S-FSDT) that provides a welcome alternative to solve this problem has been investigated. In the following, the nonlinear strain of von Kármán has been considered. In addition, in order to study the nanoscale, because of the fact that there is a difficulty with Eringen nonlocal elasticity for considering nano materials behavior when it will be applied on the nonlocal stress resultants in deriving of governing equations, because of presence of variable of nonlocal parameter, so, the modified couple stress effect has been employed in the research. Moreover, the analytical solution is used to solve the stability equations. In the end, the effects of different parameters such as; changes in the length scale parameter, external electric voltage, aspect ratio, thermal environment influences and boundary effects of edges in various conditions under in-plane shear loads have been demonstrated.

2. Formulation

A rectangular piezoelectric nanoplate is considered with thickness h, the length L_x, and the width L_y as shown in Fig.1. Of the many shear deformable plate theories proposed over the years, the FSDT is fundamentally simpler to adopt for modelling the shear deformation behavior of plates. FSDT, are widely in use, even today, because of its simplicity. It is now well-known

that in plate analysis, shear deformation effects become important not only for thick plates but even for thin plates [25]. As classical plate theory (CPT) does not take into account shear effects, many theories got evolved to address the deficiency. According to the FSDT, the following displacement field can be expressed as [22]:

$$\begin{Bmatrix} U(x,y,z) \\ V(x,y,z) \\ W(x,y,z) \end{Bmatrix} = \begin{Bmatrix} u(x,y)+z\varphi(x,y) \\ v(x,y)+z\psi(x,y) \\ w(x,y) \end{Bmatrix} \tag{1a-c}$$

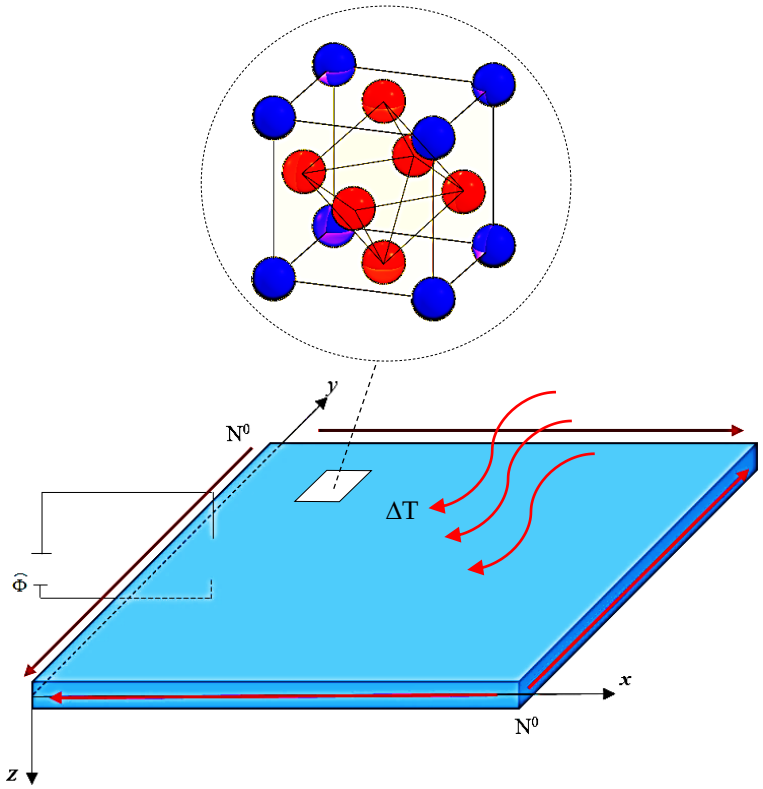

Fig. 1. Schematic picture of a rectangular piezoelectric nanoplate in thermal environment

where u, v and w are the displacement components along x, y and z directions, respectively. Moreover, φ and ψ are the rotational displacement about the y and x directions, respectively. In this theory, the shear stresses in the thickness direction is a constant value which in fact is not true. But, in the S-FSDT theory it is assumed that the transverse displacement (w) is divided into the bending component (w_b) and the shear component (w_s) which means that [26]:

$$w = w(bending) + w(shear) \tag{2}$$

Also, the rotation variable in the S-FSDT is expressed in terms of the bending component only:

$$\begin{Bmatrix} \varphi \\ \psi \end{Bmatrix} = \begin{Bmatrix} -\dfrac{\partial w_b}{\partial x} \\ -\dfrac{\partial w_b}{\partial y} \end{Bmatrix} \tag{3}$$

With implementation Eqs. (2, 3) into Eq. (1) the S-FSDT displacement field can be written as follows:

$$\begin{Bmatrix} U(x,y,z) \\ V(x,y,z) \\ W(x,y,z) \end{Bmatrix} = \begin{Bmatrix} u(x,y)-z\dfrac{\partial w_b}{\partial x} \\ v(x,y)-z\dfrac{\partial w_b}{\partial y} \\ w_b(x,y)+w_s(x,y) \end{Bmatrix} \tag{4}$$

In recent years, various size dependent continuum theories such as couple stress theory, modified couple stress theory, strain gradient theory and nonlocal elasticity theory have proposed. These theories are comprised of information about the inter-atomic forces and internal lengths. Among these theories, nonlocal elasticity theory of Eringen has been widely applied. But in this theory, we cannot find a unique result, since we have to use variable nonlocal parameter. The classical couple stress theory is one of the higher order continuum theories, which contains two additional material length scale parameters besides the classical constants for an elastic material, elaborated by Mindlin and Tieresten [27], Toupin [28], and Koiter [29]. In fact, couple stress theory is a special case of Micropolar theory proposed by Cosserat brothers [30]. Newly, a modified couple stress theory, which contains only one additional material length scale parameter in addition to the classical material constants, was proposed by Yang et al. [31]. The modified couple stress theory is more useful than classical one due to symmetric couple stress tensor. According to this higher-order continuum theory and using the Hamilton's principle, the governing equations as well as the related boundary conditions along the edges of the rectangular piezoelectric nanoplate can be derived. The equations of the total potential energy (V) are expressed as:

$$V = S + \Omega \tag{5}$$

Here S is strain energy and Ω is work done by external loads. The virtual strain energy can be calculated as:

$$\delta S = \iiint_v \left(\sigma_{ij} \delta \varepsilon_{ij} + m_{ij} \delta \chi_{ij} - D_k \delta E_k \right) dV = 0 \tag{6}$$

where σ_{ij}, ε_{ij}, m_{ij}, χ_{ij}, D_k, E_k, are stress tensor, strain tensor, deviatoric part of the couple stress tensor, symmetric curvature tensor, electric displacement and electric field, respectively [32-34].

$$\sigma_{ij} = C_{ijkl}\varepsilon_{kl} - e_{kij}E_k - \lambda_{ij}\Delta T\,,\quad D_i = e_{ikl}\varepsilon_{kl} + \kappa_{ij}E_k + p_i\Delta T \tag{7}$$

$$\varepsilon_{ij} = \frac{1}{2}\left(\frac{\partial u_i}{\partial x_j} + \frac{\partial u_j}{\partial x_i} + \frac{\partial u_k}{\partial x_i}\frac{\partial u_k}{\partial x_j} \right) \tag{8}$$

$$m_{ij} = 2G_{xy} l^2 \chi_{ij} \tag{9}$$

$$\chi_{ij} = \frac{1}{2}\left(\frac{\partial \theta_i}{\partial x_j} + \frac{\partial \theta_j}{\partial x_i} \right);\ \theta_i = \frac{1}{2} e_{ijk} U_{k,j} \tag{10}$$

where l is a material length scale parameter that is related to size effect, and θ is the rotation vector. Also, C_{ijkl}, e_{kij}, κ_{ij}, λ_{ij}, p_i are elastic constant, piezoelectric constant, dielectric constant, thermal moduli and pyroelectric constant, respectively. The tensors associated in the displacement field in Eqs. (7-10) are:

$$\begin{Bmatrix} \varepsilon_{xx} \\ \varepsilon_{yy} \\ \gamma_{yz} \\ \gamma_{xz} \\ \gamma_{xy} \end{Bmatrix} = \begin{Bmatrix} \dfrac{\partial u}{\partial x} - z\dfrac{\partial^2 w_b}{\partial x^2} + \dfrac{1}{2}\left(\dfrac{\partial w_b}{\partial x}\right)^2 + \dfrac{1}{2}\left(\dfrac{\partial w_s}{\partial x}\right)^2 + \dfrac{\partial w_b}{\partial x}\dfrac{\partial w_s}{\partial x} \\ \dfrac{\partial v}{\partial y} - z\dfrac{\partial^2 w_b}{\partial y^2} + \dfrac{1}{2}\left(\dfrac{\partial w_b}{\partial y}\right)^2 + \dfrac{1}{2}\left(\dfrac{\partial w_s}{\partial y}\right)^2 + \dfrac{\partial w_b}{\partial y}\dfrac{\partial w_s}{\partial y} \\ \dfrac{\partial w_s}{\partial y} \\ \dfrac{\partial w_s}{\partial x} \\ \left(\dfrac{\partial u}{\partial y} + \dfrac{\partial v}{\partial x}\right) - 2z\dfrac{\partial^2 w_b}{\partial x \partial y} + \left(\dfrac{\partial w_b}{\partial x} + \dfrac{\partial w_s}{\partial x}\right)\left(\dfrac{\partial w_b}{\partial y} + \dfrac{\partial w_s}{\partial y}\right) \end{Bmatrix} \tag{11a-e}$$

$$\begin{Bmatrix}\chi_x\\ \chi_y\\ \chi_{xy}\\ \chi_{xz}\\ \chi_{yz}\end{Bmatrix}=\begin{Bmatrix}\frac{1}{2}\left(2\frac{\partial^2 w_b}{\partial x\partial y}+\frac{\partial^2 w_s}{\partial x\partial y}\right)\\ \frac{1}{2}\left(-2\frac{\partial^2 w_b}{\partial x\partial y}-\frac{\partial^2 w_s}{\partial x\partial y}\right)\\ \frac{1}{4}\left(-2\frac{\partial^2 w_b}{\partial x^2}+2\frac{\partial^2 w_b}{\partial y^2}-\frac{\partial^2 w_s}{\partial x^2}+\frac{\partial^2 w_s}{\partial y^2}\right)\\ \frac{1}{4}\left(\frac{\partial^2 v}{\partial x^2}-\frac{\partial^2 u}{\partial x\partial y}\right)\\ \frac{1}{4}\left(-\frac{\partial^2 u}{\partial y^2}+\frac{\partial^2 v}{\partial x\partial y}\right)\end{Bmatrix} \tag{12a-e}$$

$$e_{kij}=\begin{bmatrix}0 & 0 & \hat{e}_{31}\\ 0 & 0 & \hat{e}_{31}\\ \hat{e}_{15} & 0 & 0\\ 0 & \hat{e}_{15} & 0\\ 0 & 0 & 0\end{bmatrix},\ e_{ikl}=e_{kij}{}^{T},\quad p_k=\begin{Bmatrix}p_1\\ p_2\\ p_3\end{Bmatrix} \tag{13a-c}$$

To confirm the Maxwell equation, the distribution of external electric potential for the present nanoplate model is assumed as a combination of a cosine and linear variation [34-36].

$$\Phi\ (x,y,z)=-\cos(\beta z)\Phi\ (x,y)+\frac{2zV_0}{h} \tag{14}$$

where $\beta=\pi/h$; $\Phi\ (x,y)$ is the spatial of the electric potential in the mid-plane of the nanoplate, and V_0 is the external electric voltage. Then, the components of electric field can be written as:

$$E_k=\begin{Bmatrix}E_x=-\frac{\partial\Phi}{\partial x}\\ E_y=-\frac{\partial\Phi}{\partial y}\\ E_z=-\frac{\partial\Phi}{\partial z}\end{Bmatrix}=\begin{Bmatrix}\cos(\beta z)\frac{\partial\Phi}{\partial x}\\ \cos(\beta z)\frac{\partial\Phi}{\partial y}\\ -\beta\sin(\beta z)\Phi-\frac{2V_0}{h}\end{Bmatrix} \tag{15a-c}$$

Using the principle of minimum potential energy ($\delta V=0$) the nonlinear constitutive equations are derived as:

$$
[\delta V]=0:\begin{bmatrix}
\dfrac{\partial N_{x}}{\partial x}+\dfrac{\partial N_{xy}}{\partial y}+\dfrac{1}{4}\dfrac{\partial^2 Y_{xz}}{\partial x\partial y}+\dfrac{1}{4}\dfrac{\partial Y_{yz}}{\partial y^2}=0\\
\dfrac{\partial N_{xy}}{\partial x}+\dfrac{\partial N_{y}}{\partial y}-\dfrac{1}{4}\dfrac{\partial^2 Y_{xz}}{\partial x^2}-\dfrac{1}{4}\dfrac{\partial^2 Y_{yz}}{\partial x\partial y}=0\\
\dfrac{\partial Q_{x}}{\partial x}+\dfrac{\partial Q_{y}}{\partial y}+N_{xx}\left(\dfrac{\partial^2 w_s}{\partial x^2}+\dfrac{\partial^2 w_b}{\partial x^2}\right)+N_{yy}\left(\dfrac{\partial^2 w_s}{\partial y^2}+\dfrac{\partial^2 w_b}{\partial y^2}\right)+2N_{xy}\left(\dfrac{\partial^2 w_s}{\partial x\partial y}+\dfrac{\partial^2 w_b}{\partial x\partial y}\right)-\dfrac{\partial^2 Y_{xx}}{\partial x\partial y}+\dfrac{1}{2}\dfrac{\partial^2 Y_{yy}}{\partial x\partial y}\\
-\dfrac{1}{4}\dfrac{\partial^2 Y_{xy}}{\partial y^2}+\dfrac{1}{4}\dfrac{\partial^2 Y_{xy}}{\partial x^2}=0\\
-\dfrac{\partial^2 M_{x}}{\partial x^2}-2\dfrac{\partial^2 M_{xy}}{\partial x\partial y}-\dfrac{\partial^2 M_{y}}{\partial y^2}+N_{xx}\left(\dfrac{\partial^2 w_s}{\partial x^2}+\dfrac{\partial^2 w_b}{\partial x^2}\right)+N_{yy}\left(\dfrac{\partial^2 w_s}{\partial y^2}+\dfrac{\partial^2 w_b}{\partial y^2}\right)+2N_{xy}\left(\dfrac{\partial^2 w_s}{\partial x\partial y}+\dfrac{\partial^2 w_b}{\partial x\partial y}\right)-2\dfrac{\partial^2 Y_{xx}}{\partial x\partial y}\\
+\dfrac{\partial^2 Y_{yy}}{\partial x\partial y}-\dfrac{1}{2}\dfrac{\partial^2 Y_{xy}}{\partial y^2}+\dfrac{1}{2}\dfrac{\partial^2 Y_{xy}}{\partial x^2}=0\\
\int_{-h/2}^{h/2}\left[\dfrac{\partial \overline{D_x}}{\partial x}\cos(\beta z)+\dfrac{\partial \overline{D_y}}{\partial y}\cos(\beta z)+\overline{D_z}\beta\sin(\beta z)\right]dz=0
\end{bmatrix}
\tag{16a-e}
$$

N_i, M_i and Q_i *(i= x, y, xy)* and Y_{ij} *(i= x, y, xy)* are stress resultants and non-zero curvature resultants, respectively, as follows:

$$(N_x,N_y,N_{xy})=\int_{-h/2}^{h/2}\left(\sigma_x,\sigma_y,\sigma_{xy}\right)dz \tag{17a}$$

$$(M_x,M_y,M_{xy})=\int_{-h/2}^{h/2}\left(\sigma_x,\sigma_y,\sigma_{xy}\right)zdz \tag{17b}$$

$$\left(Q_x,Q_y\right)=\int_{-h/2}^{h/2}\left(\sigma_{xz},\sigma_{yz}\right)dz \tag{17c}$$

$$\begin{Bmatrix}Y_{xx}\\Y_{yy}\\Y_{xy}\\Y_{xz}\\Y_{yz}\end{Bmatrix}=\int_{-h/2}^{h/2}\begin{Bmatrix}m_{xx}\\m_{yy}\\m_{xy}\\m_{xz}\\m_{yz}\end{Bmatrix}dz \tag{18}$$

$$\begin{Bmatrix}D_x\\D_y\\D_z\end{Bmatrix}=\int_{-h/2}^{h/2}\begin{Bmatrix}D_x\cos(\beta z)\\D_y\cos(\beta z)\\D_z\beta\sin(\beta z)\end{Bmatrix}dz=\begin{Bmatrix}E_{15}\dfrac{\partial w_s}{\partial x}+X_{11}\dfrac{\partial\Phi}{\partial x}+\dfrac{2p_1\Delta T}{\beta}\sin\left(\dfrac{\beta h}{2}\right)\\E_{15}\dfrac{\partial w_s}{\partial y}+X_{11}\dfrac{\partial\Phi}{\partial y}+\dfrac{2p_1\Delta T}{\beta}\sin\left(\dfrac{\beta h}{2}\right)\\-E_{31}\dfrac{\partial^2 w_b}{\partial x^2}-E_{31}\dfrac{\partial^2 w_b}{\partial y^2}-X_{33}\Phi\end{Bmatrix} \tag{19}$$

in which D_i is generated flux. The coefficients in Eq. 19 can be expressed respectively.

$$\begin{Bmatrix}E_{31}\\E_{15}\\X_{11}\\X_{33}\end{Bmatrix}=\int_{-h/2}^{h/2}\begin{Bmatrix}\widehat{e}_{31}\beta z\sin(\beta z)\\\widehat{e}_{15}\cos(\beta z)\\\kappa_{11}\cos^2(\beta z)\\\kappa_{33}\beta^2\sin^2(\beta z)\end{Bmatrix}dz \tag{20}$$

In the following, the governing equations (Eq. 16) for the rectangular piezoelectric nanoplate can be rewritten:

$$N_{x,x}+N_{xy,y}+\frac{1}{2}A_s\left(-\frac{\partial^4 u}{\partial x^2\partial y^2}+\frac{\partial^4 v}{\partial x^3\partial y}\right)+\frac{1}{2}A_s\left(-\frac{\partial^4 u}{\partial y^4}+\frac{\partial^4 v}{\partial x\partial y^3}\right)=0 \tag{21a}$$

$$N_{xy,x}+N_{y,y}-\frac{1}{2}A_s\left(-\frac{\partial^4 u}{\partial x^3\partial y}+\frac{\partial^4 v}{\partial x^4}\right)-\frac{1}{2}A_s\left(-\frac{\partial^4 u}{\partial x\partial y^3}+\frac{\partial^4 v}{\partial x^2\partial y^2}\right)=0 \tag{21b}$$

$$Q_{x,x}+Q_{y,y}+N_{xx}\left(\frac{\partial^2 w_b}{\partial x^2}+\frac{\partial^2 w_s}{\partial x^2}\right)+N_{yy}\left(\frac{\partial^2 w_b}{\partial y^2}+\frac{\partial^2 w_s}{\partial y^2}\right)+2N_{xy}\left(\frac{\partial^2 w_b}{\partial x\partial y}+\frac{\partial^2 w_s}{\partial x\partial y}\right)-\frac{1}{2}A_s\left(5\frac{\partial^4 w_b}{\partial x^2\partial y^2}+3\frac{\partial^4 w_s}{\partial x^2\partial y^2}\right)-$$
$$\frac{1}{4}A_s\left(\frac{\partial^4 w_b}{\partial x^4}+\frac{1}{2}\frac{\partial^4 w_s}{\partial x^4}+\frac{\partial^4 w_b}{\partial y^4}+\frac{1}{2}\frac{\partial^4 w_s}{\partial y^4}\right)=0 \tag{21c}$$

$$-M_{x,xx}-2M_{xy,xy}-M_{y,yy}+N_{xx}\left(\frac{\partial^2 w_b}{\partial x^2}+\frac{\partial^2 w_s}{\partial x^2}\right)+N_{yy}\left(\frac{\partial^2 w_b}{\partial y^2}+\frac{\partial^2 w_s}{\partial y^2}\right)+2N_{xy}\left(\frac{\partial^2 w_b}{\partial x\partial y}+\frac{\partial^2 w_s}{\partial x\partial y}\right)-\frac{5}{2}A_s\left(2\frac{\partial^4 w_b}{\partial x^2\partial y^2}+\frac{\partial^4 w_s}{\partial x^2\partial y^2}\right)$$
$$-\frac{1}{4}A_s\left(2\frac{\partial^4 w_b}{\partial x^4}+\frac{\partial^4 w_s}{\partial x^4}+2\frac{\partial^4 w_b}{\partial y^4}+\frac{\partial^4 w_s}{\partial y^4}\right)=0 \tag{21d}$$

$$\int_{-h/2}^{h/2}\left[\frac{\partial D_x}{\partial x}\cos(\beta z)+\frac{\partial D_y}{\partial y}\cos(\beta z)+D_z\beta\sin(\beta z)\right]dz=0 \tag{21e}$$

in which A_s is defined as follows:

$$A_s=\int_{-\frac{h}{2}}^{\frac{h}{2}} l^2 C_{66}\,dz \tag{22}$$

The axial and flexural rigidities of the piezoelectric nanoplate are given by:

$$A_{ij}=\int_{-\frac{h}{2}}^{\frac{h}{2}} C_{ij}\,dz\quad (i,j=1,2,4,6)\ ,\ D_{ij}=\int_{-\frac{h}{2}}^{\frac{h}{2}} C_{ij}z^2\,dz\quad (i,j=1,2,6) \tag{23a}$$

$$\begin{Bmatrix}C_{11}\\C_{12}\\C_{44}\\C_{66}\end{Bmatrix}=\begin{Bmatrix}C_{11}-\frac{C_{13}^2}{C_{33}}\\C_{12}-\frac{C_{13}^2}{C_{33}}\\C_{44}\\C_{66}\end{Bmatrix},\ \begin{Bmatrix}\widehat{e}_{31}\\\widehat{e}_{15}\\\kappa_{11}\\\kappa_{33}\end{Bmatrix}=\begin{Bmatrix}e_{31}-\frac{C_{13}e_{33}}{C_{33}}\\e_{15}\\\kappa_{11}\\\kappa_{33}+\frac{e_{33}^2}{C_{33}}\end{Bmatrix} \tag{23b}$$

$$\begin{Bmatrix}m_{xx}\\m_{yy}\\m_{xy}\\m_{xz}\\m_{yz}\end{Bmatrix}=l^2C_{66}\begin{Bmatrix}\left(2\frac{\partial^2 w_b}{\partial x\partial y}+\frac{\partial^2 w_s}{\partial x\partial y}\right)\\\left(-2\frac{\partial^2 w_b}{\partial x\partial y}-\frac{\partial^2 w_s}{\partial x\partial y}\right)\\\frac{1}{2}\left(-2\frac{\partial^2 w_b}{\partial x^2}+2\frac{\partial^2 w_b}{\partial y^2}-\frac{\partial^2 w_s}{\partial x^2}+\frac{\partial^2 w_s}{\partial y^2}\right)\\\frac{1}{2}\left(\frac{\partial^2 v}{\partial x^2}-\frac{\partial^2 u}{\partial x\partial y}\right)\\\frac{1}{2}\left(-\frac{\partial^2 u}{\partial y^2}+\frac{\partial^2 v}{\partial x\partial y}\right)\end{Bmatrix},\ \kappa_{ij}=\begin{bmatrix}\widehat{\kappa_{11}}&0&0\\0&\widehat{\kappa_{11}}&0\\0&0&\widehat{\kappa_{33}}\end{bmatrix} \tag{23c}$$

In Eq. (23a), A_{ij} and D_{ij} are extensional stiffness and extension-bending coupling matrix, respectively. The stress resultants in Eq. (17) in displacement field by using Eq.23 and substituting in Eq.17 are defined as:

$$\begin{bmatrix} N_{xx} \\ N_{yy} \\ N_{xy} \\ M_{xx} \\ M_{yy} \\ M_{xy} \\ Q_y \\ Q_x \end{bmatrix}^{Total} = \begin{bmatrix} A_{11} & A_{12} & 0 & 0 & 0 & 0 & 0 & 0 \\ A_{21} & A_{22} & 0 & 0 & 0 & 0 & 0 & 0 \\ 0 & 0 & A_{66} & 0 & 0 & 0 & 0 & 0 \\ 0 & 0 & 0 & D_{11} & D_{12} & 0 & 0 & 0 \\ 0 & 0 & 0 & D_{21} & D_{22} & 0 & 0 & 0 \\ 0 & 0 & 0 & 0 & 0 & D_{66} & 0 & 0 \\ 0 & 0 & 0 & 0 & 0 & 0 & A_{44} & 0 \\ 0 & 0 & 0 & 0 & 0 & 0 & 0 & A_{44} \end{bmatrix} \times \begin{bmatrix} \frac{\partial u}{\partial x} + \frac{1}{2}\left(\frac{\partial w_b}{\partial x}\right)^2 + \frac{1}{2}\left(\frac{\partial w_s}{\partial x}\right)^2 + \frac{\partial w_b}{\partial x}\frac{\partial w_s}{\partial x} \\ \frac{\partial v}{\partial y} + \frac{1}{2}\left(\frac{\partial w_b}{\partial y}\right)^2 + \frac{1}{2}\left(\frac{\partial w_s}{\partial y}\right)^2 + \frac{\partial w_b}{\partial y}\frac{\partial w_s}{\partial y} \\ \frac{\partial u}{\partial y} + \frac{\partial v}{\partial x} + \left(\frac{\partial w_b}{\partial x} + \frac{\partial w_s}{\partial x}\right)\left(\frac{\partial w_b}{\partial y} + \frac{\partial w_s}{\partial y}\right) \\ -\frac{\partial^2 w_b}{\partial x^2} \\ -\frac{\partial^2 w_b}{\partial y^2} \\ -\frac{\partial^2 w_b}{\partial x \partial y} \\ \frac{\partial w_s}{\partial y} \\ \frac{\partial w_s}{\partial x} \end{bmatrix}^{Mech} + \begin{Bmatrix} 2\widehat{e}_{31}V_0 \\ 2\widehat{e}_{31}V_0 \\ 0 \\ E_{31}\Phi \\ E_{31}\Phi \\ 0 \\ -E_{15}\frac{\partial \Phi}{\partial y} \\ -E_{15}\frac{\partial \Phi}{\partial x} \end{Bmatrix}^{Elec} - \begin{Bmatrix} \widehat{\lambda_{11}h}\Delta T \\ \widehat{\lambda_{11}h}\Delta T \\ 0 \\ 0 \\ 0 \\ 0 \\ 0 \\ 0 \end{Bmatrix}^{Ther} \tag{24}$$

$$\begin{Bmatrix} p_1 \\ p_3 \end{Bmatrix} = \begin{Bmatrix} p_1 \\ p_3 + \frac{e_{33}\lambda_{33}}{C_{33}} \end{Bmatrix}; \ \lambda_{11} = \lambda_{11} - \frac{C_{13}\lambda_{33}}{C_{33}} \tag{25}$$

where $N_{xy} = -N^0$ is critical shear in-plane load in buckling conditions. Inserting Eqs. (18, 19) and (24, 25) in Eq. (21), and also with considering the pre-buckling conditions the thermo-electro-mechanical stability equations in the form of displacement components and based on S-FSDT also including couple stress effect are expressed as follows:

$$A_{44}\left(\frac{\partial^2 w_s}{\partial x^2} + \frac{\partial^2 w_s}{\partial y^2}\right) - 2N^0\left(\frac{\partial^2 w_b}{\partial x \partial y} + \frac{\partial^2 w_s}{\partial x \partial y}\right) + \left(2\widehat{e}_{31}V_0 - \lambda_{11}h\Delta T\right)\times\left(\frac{\partial^2 w_b}{\partial x^2} + \frac{\partial^2 w_s}{\partial x^2}\right) + \left(2\widehat{e}_{31}V_0 - \lambda_{11}h\Delta T\right)\times\left(\frac{\partial^2 w_b}{\partial y^2} + \frac{\partial^2 w_s}{\partial y^2}\right) - E_{15}\frac{\partial^2 \Phi}{\partial x^2} - E_{15}\frac{\partial^2 \Phi}{\partial y^2}$$
$$-A_s\left[\frac{1}{2}\left(5\frac{\partial^4 w_b}{\partial x^2 \partial y^2} + 3\frac{\partial^4 w_s}{\partial x^2 \partial y^2}\right) - \frac{1}{4}\left(\frac{\partial^4 w_b}{\partial x^4} + \frac{1}{2}\frac{\partial^4 w_s}{\partial x^4} + \frac{\partial^4 w_b}{\partial y^4} + \frac{1}{2}\frac{\partial^4 w_s}{\partial y^4}\right)\right] = 0$$

$$D_{11}\frac{\partial^4 w_b}{\partial x^4} + 2\left(D_{12} + D_{66}\right)\frac{\partial^4 w_b}{\partial x^2 \partial y^2} + D_{22}\frac{\partial^4 w_b}{\partial y^4} - 2N^0\left(\frac{\partial^2 w_b}{\partial x \partial y} + \frac{\partial^2 w_s}{\partial x \partial y}\right) + \left(2\widehat{e}_{31}V_0 - \lambda_{11}h\Delta T\right)\times\left(\frac{\partial^2 w_b}{\partial x^2} + \frac{\partial^2 w_s}{\partial x^2}\right) + \left(2\widehat{e}_{31}V_0 - \lambda_{11}h\Delta T\right)\times\left(\frac{\partial^2 w_b}{\partial y^2} + \frac{\partial^2 w_s}{\partial y^2}\right)$$
$$+E_{31}\frac{\partial^2 \Phi}{\partial x^2} + E_{31}\frac{\partial^2 \Phi}{\partial y^2} - A_s\left[\frac{5}{2}\left(2\frac{\partial^4 w_b}{\partial x^2 \partial y^2} + \frac{\partial^4 w_s}{\partial x^2 \partial y^2}\right) - \frac{1}{4}\left(2\frac{\partial^4 w_b}{\partial x^4} + \frac{\partial^4 w_s}{\partial x^4} + 2\frac{\partial^4 w_b}{\partial y^4} + \frac{\partial^4 w_s}{\partial y^4}\right)\right] = 0$$

$$E_{15}\left(\frac{\partial^2 w_s}{\partial x^2} + \frac{\partial^2 w_s}{\partial y^2}\right) - E_{31}\left(\frac{\partial^2 w_b}{\partial x^2} + \frac{\partial^2 w_b}{\partial y^2}\right) + X_{11}\left(\frac{\partial^2 \Phi}{\partial x^2} + \frac{\partial^2 \Phi}{\partial y^2}\right) - X_{33}\Phi = 0$$

(26a-c)

3. Analytical solution

In this section, a closed-form solution of the stability equations in order to obtain critical force of a piezoelectric nanoplate with simply-supported (S), clamped (C), and free (F) edges or combinations of these boundary conditions is presented, in which they are given as [37-39]:

Simply-supported (S):

$w_b = w_s = \Phi = Mx = 0$; *at* $x = 0, Lx$

$w_b = w_s = \Phi = My = 0$; *at* $y = 0, Ly$

Clamped (C):

$w_b = w_s = \Phi = 0$; *at* $x = 0, Lx$ *and* $y = 0, Ly$

Free edges (F):

$M_x = M_{xy} = Q_{xz} = 0$; *at* $x = 0, Lx$

$M_y = M_{xy} = Q_{yz} = 0$; *at* $y = 0, Ly$

The following expansions have been assumed to satisfy the above mentioned boundary conditions:

Free edges (F): $X_i = \left[\sin^2(\alpha_i x_i)+1\right]\cos^2(\alpha_i x_i)$; *i=1,2* (27a)

Clamped (C): $X_i = \sin^2(\alpha_i x_i)$; *i=1,2* (27b)

Simply-supported (S): $X_i = \sin(\alpha_i x_i)$; *i=1,2* (27c)

where *m* and *n* are the half wave numbers, $\alpha_1 = m\pi/Lx$, $\alpha_2 = n\pi/Ly$; $x_1=x$, $x_2=y$ or terms used in the *x* and *y* direction to represent the displacement functions. We use the displacement function in the following form:

$w_k(x,y) = W_k \times X_i \times X_j$; *k=s,b; i=1,2 ; j=1,2* (28a)

$\Phi(x,y) = \Phi_m \times X_i \times X_j$; *i=1,2 ; j=1,2* (28b)

Substituting the expression of w_k, Φ in Eq. (26) the explicit relation can be obtained for buckling loads with various boundary conditions. The stability equations and closed-form boundary conditions yield a set of following algebraic equations:

$$\left\{\begin{bmatrix} p_{11} & p_{12} & p_{13} \\ p_{21} & p_{22} & p_{23} \\ p_{31} & p_{32} & p_{33} \end{bmatrix} - N^0 \begin{bmatrix} r_{11} & r_{12} & r_{13} \\ r_{21} & r_{22} & r_{23} \\ r_{31} & r_{32} & r_{33} \end{bmatrix}\right\} \begin{Bmatrix} W_b \\ W_s \\ \Phi_m \end{Bmatrix} = 0 \tag{29}$$

p_{ij} (i,j=1,2,3) and r_{ij} (i,j=1,2,3) are coefficients of constants terms. To find a solution for the above equation, the determinant of the matrix of coefficients must be set to zero. By doing so, the critical load is determined.

5. Numerical results

The results validation and comparison with other research results should obviously be carried out before investigating various parameters of this article. Because of this fact that there are not any available papers in the field of shear buckling of piezoelectric nanoplates, therefore, Tables 1 and 2 which were in nanoplates field are examined in order to compare and validate this formulation results with those of other articles. In order for the results to be compared in Tables 1 and 2, [19] and [40] were employed while their results are obtained using first order shear deformation theory, differential quadrature method (DQM), as well as Eringen nonlocal elasticity theory. Ref. [41] is added for further confirmation due to the minor errors in the numerical solutions, and its results are obtained through molecular dynamics solution. Therefore, observing numerical solution alone does not enable us to ascertain the fact that the present results are validated due to the difference between the results in both cases. However, by examining Tables 1 and 2, one can strongly express that the modified first order shear deformation theory (S-FSDT) results appropriately correspond to the molecular dynamic results. Since the solution is an exact one, this proximity of the results clearly confirms this premise that accurate and appropriate results are obtained by combining the simplified first order shear deformation theory and an analytical solution. Comparing the results shown in Table 1 with 2 confirms that the removal of the shear stress correction factors in plates affects the critical load results. Because, the difference generated in the contractual FSDT by employing this factor when compared with the accurate results, is removed in the S-FSDT. According to Tables 1 and 2 the thinner we assume the plate, the closer the results become to the FSDT results and numerical solution, while their accuracy decreases; because, FSDT is not applicable to analyze thin plates and the classical plate theory (CPT) is more applicable in this case.

Table 1. Comparison of results for critical biaxial buckling load for single-layered graphene sheet and all edges simply supported obtained from DQ method [19, 40], and molecular dynamics simulation [41].

Table 2. Comparison of the present results with those of DQ method [38] and molecular dynamics (MD) simulation [41] for different aspect ratios of orthotropic single-layered graphene sheets under uniform biaxial compression.

E=1Tpa, υ=0.3, Lx/Ly=1, k_1=1, k_2=1, k_s=5/6, μ=1.81nm^2, l=8.5h (Has freely been chosen), SSSS.

Table 1.

Critical buckling load (*Pa.m*)				
S-FSDT, Present study	FSDT-DQM [19]	FSDT-DQM [40]	MD results [41]	Lx=Ly (*nm*)
1.0835	1.0749	1.0809	1.0837	4.99
0.6538	0.6523	0.6519	0.6536	8.080
0.4330	0.4356	0.4350	0.4331	10.77
0.2615	0.2645	0.2639	0.2609	14.65
0.1720	0.1751	0.1748	0.1714	18.51
0.1198	0.1239	0.1237	0.1191	22.35
0.0896	0.0917	0.0914	0.0889	26.22
0.0696	0.0707	0.0705	0.0691	30.04
0.0559	0.0561	0.0560	0.0554	33.85
0.0454	0.0453	0.0451	0.0449	37.81

Table 2.

Critical buckling load (*Pa.m*)			
FSDT-DQM [40]	MD results [41]	S-FSDT, Present study	Lx/Ly
0.5115	0.5101	0.5105	0.5
0.5715	0.5693	0.5698	0.75
0.6622	0.6595	0.6599	1.25
0.7773	0.7741	0.7747	1.5
1.0222	1.0183	1.0180	1.75
1.1349	1.1297	1.1301	2

Table 3. Mechanical and Electrical properties of the piezoelectric nanoplate [34]

A Piezoelectric Nanoplate	*C_{11}=132Gpa, C_{12}=71Gpa, C_{13}=73Gpa, C_{33}=115Gpa, C_{44}=26Gpa, C_{66}=30.5Gpa, e_{31}=-4.1 C/m^2, e_{15}=10.5 C/m^2, e_{33}=14.1 C/m^2, κ_{11}=5.841e-9 C/Vm, κ_{33}=7.124e-9 C/Vm, λ_{11}=4.738e5 N/m^{2}K, λ_{33}=4.529e5 N/m^{2}K, p_1=0.25e-4 C/m^{2}K, p_3=0.25e-4 C/m^{2}K*

Fig.2 shows *m* and *n* variations for square and rectangular Nano-Piezoelectric-Sheets. It is clear that results are not accurate before *m=n=30*, but after *m=n>40* the critical shear loads almost converge to the point that *m* and *n* variations have no effect on

critical shear load at $m=n>50$. Therefore, the results at $m=n=50$ are convenient for extracting the critical shear load of piezoelectric nano-sheets from.

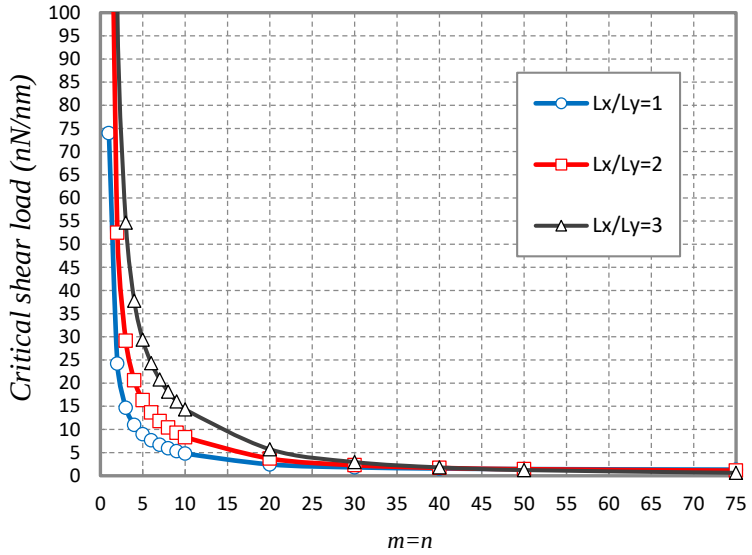

Fig. 2. The effect of aspect ratio (Lx/Ly) versus wave numbers *($Ly=30h$, $l=h$, $V_0=0.1$ V, SSSS, $\Delta T=500$ K)*

In order to study the effect of length scale on different boundary conditions, Fig.3a was examined. It was found that with a more flexible boundary condition critical load results decrease, which means that the maximum critical shear load occurs with clamped boundary conditions providing the minimum flexibility. The length scale parameter has more effect for SFSF and SSSS. The reason is gotten from more difference of critical shear load results between both of boundary conditions while length scale parameter is increased.

On the other hand, the effect of nanosize has been considered by using length scale parameter which shows the effect of small size. By looking at Fig. 3b, it is shown that by increasing l parameter the critical load will be greater. If we select l=0, in fact a macro plate will be taken into account. On the whole, it can be concluded that by considering a nanosize plate ($l\neq0$) the greater values of critical load will be resulted. Although the amount of l parameter must be found in laboratory by investigating many conditions, the values used in the figures are nondimensional. Another impressive results could be differences among critical loads developed from various voltage, that is, whatever the value of l will be larger, the difference will be greater.

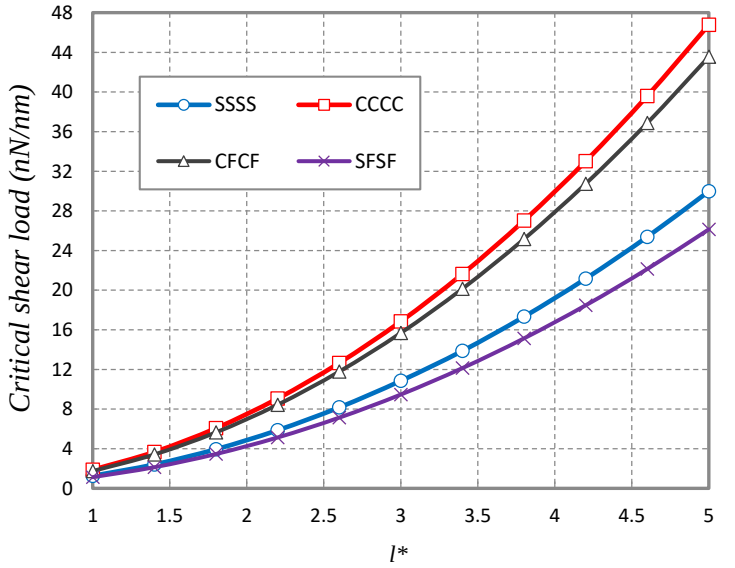

Fig. 3a. The length scale parameter versus different boundary conditions ($Lx=Ly=30h$, $l^*=l/h$, $V_0=0.05$ V, $\Delta T=500$ K)

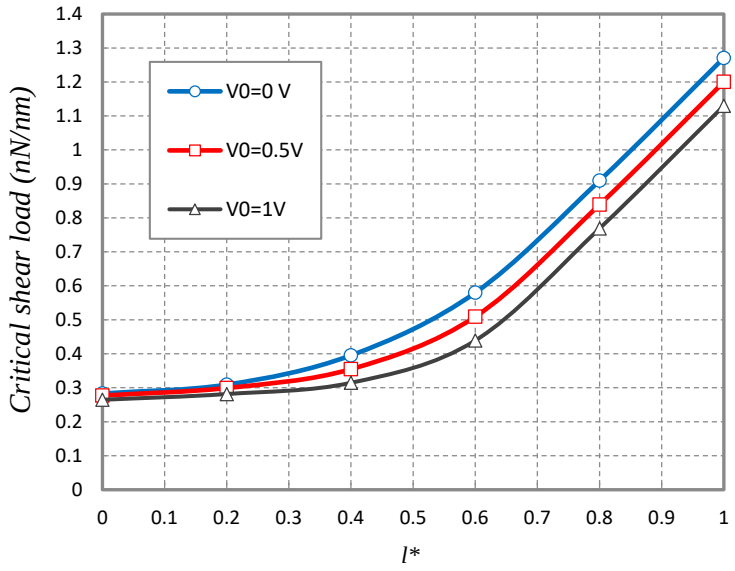

Fig. 3b. Impact of length scale parameter on critical shear load in macro and nano plates (*Lx=Ly=30h, l*=l/h, SSSS, ΔT=500 K)*

Fig. 4 is plotted to examine the effect of external electric voltage applied to the piezoelectric nano-sheet versus the length to width ratio and it is extracted for simply supported boundary condition. Fig.4 presents that with simply supported boundary condition, critical shear load decreases with increasing external voltage, but the effect of external voltage on critical load is negligible. Furthermore, it is evident that with an increased length to width ratio the critical shear load decreases and external voltage becomes more effective. The difference in results of the diagrams proves the statement.

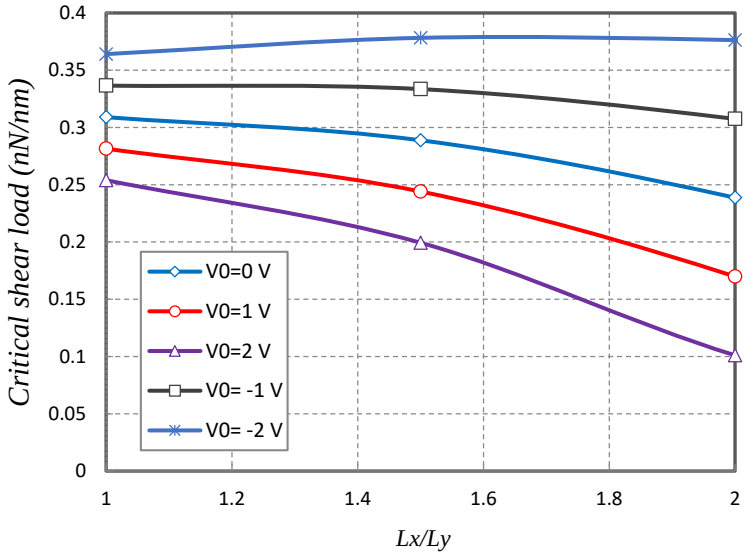

Fig. 4. The effect of aspect ratio (*Lx/Ly*) parameter versus external electric voltage (*Ly=30h, l=0.2h, SSSS, ΔT=300 K*)

Fig.5 shows the direct effect of external voltage on critical shear load. Results were extracted for CFCF and CCCC boundary conditions and suggest that the effect of external voltage on critical shear load is negligible. On the other hand, with the external voltage increased, minute differences appear in critical shear load results, showing the effect of external voltage on critical shear load to be negligible. In fact, the critical shear load occurring on the piezoelectric nano-sheet due to external electric current is insignificant. Also, it is clearly, with increasing external voltage, the critical shear load is declined in CFCF and vice versa in CCCC will rise.

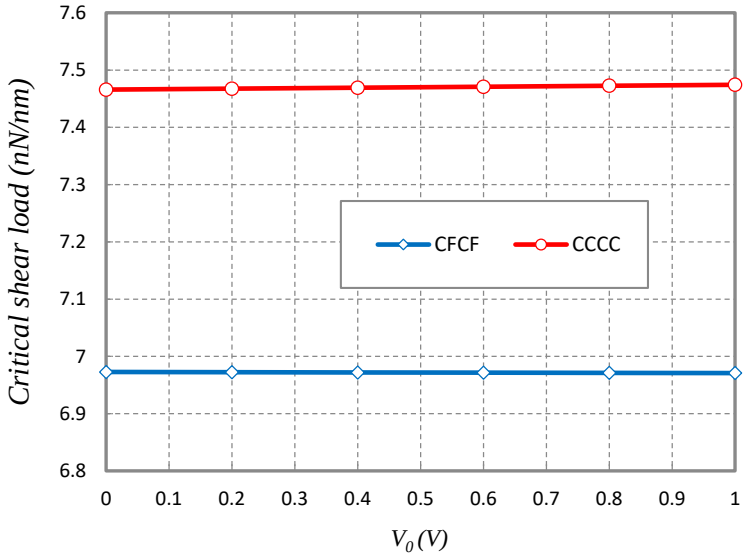

Fig. 5. The effect of different boundary conditions versus external electric voltage (*Ly=30h, l=2h, ΔT=300 K*)

Fig. 6 displays the effects of the temperature rise ΔT (K) on the critical shear results of the piezoelectric nanoplates. The temperature rise will result in a slight decrease on the critical shear loads. However, like the electric voltage, the temperature change has very limited influences on the critical shear behaviors of the piezoelectric nanoplate. Even the temperature rise varies from 300 K to 500 K, there are merely minor variations that can be found in the critical shear load. Such phenomenon is the result of that piezoelectric nanoplate possesses a small thermal modulus, which does not transform the temperature into stress in the body effectively. If we alter the piezoelectric material to another one with large thermal modulus, it is predictably that the temperature rise can also become a sensitive factor on the buckling behavior.

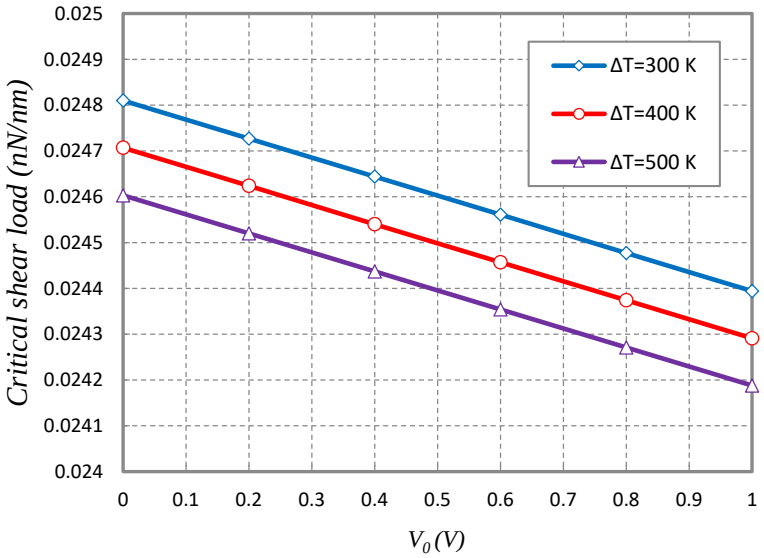

Fig. 6. The effect of thermal environment versus external electric voltage (*Ly=15h, l=0.1h, CFCF*)

6. Conclusions

This study investigated the shear buckling of the piezoelectric nanoplate under external electrical voltage in thermal environment. For this purpose, a simplified first order shear deformation theory was employed to obtain the governing equations by taking into account the von Kármán nonlinear strains. The impact of nanoscale was investigated by using modified couple stress theory. Moreover, an analytical solution was used to extract the results by changing various parameters. In conclusion, some of the important results achieved from the present study are as follows:

* The length scale impact on the results of any boundary conditions increases with an increase in *l* parameters.

* The effect of external electric voltage on the critical shear load is more than room temperature effects.

* With increasing aspect ratio the critical shear load decreases and external electric voltage becomes more impressive.

* By considering piezoelectric nanoplates, it is proved that the temperature rise cannot become a sensitive factor on the buckling behavior.

* The length scale parameter has more effect for more flexible boundary conditions than others.

* By considering nanosize, the consideration results in much bigger critical load versus macro plate.

References

[1] G., Ciofani, A., Menciassi, Piezoelectric Nanomaterials for Biomedical Applications, DOI 10.1007/978-3-642-28044-3, Springer-Verlag, Berlin Heidelberg, (2012).

[2] S.B., Lang, Guide to the literature of piezoelectricity and pyroelectricity 28. Ferroelectrics, 361 (2007) 130–216.

[3] Z.-G., Ye, et al.: Handbook of dielectric, piezoelectric and ferroelectric materials: synthesis, properties and applications. Woodhead Pub., Maney Pub. on behalf of The Institute of Materials, Minerals & Mining, CRC Press, Boca Raton (2008).

[4] G.H., Haertling, Ferroelectric Ceramics: History and Technology. Journal of the American Ceramic Society, 82 (1999) 797–818.

[5] S.C., Pradhan, T., Murmu, Small scale effect on the buckling analysis of single-layered graphene sheet embedded in an elastic medium based on nonlocal plate theory, Physica E, 42 (2010) 1293–1301.

[6] Ö. Civalek, Ç. Demir, B. Akgöz, Free Vibration and Bending Analysis of Cantilever Microtubules Based On Nonlocal Continuum Model, Math. & Comput. Appl., 15 (2010) 289–298.

[7] B. Akgöz, Ö. Civalek, Strain gradient elasticity and modified couple stress models for buckling analysis of axially loaded micro-scaled beams, Int. Jour. of Eng. Sci., 49 (2011) 1268–1280.

[8] P. Malekzadeh, A.R. Setoodeh, A.A. Beni, Small scale effect on the thermal buckling of orthotropic arbitrary straight-sided quadrilateral nanoplates embedded in an elastic medium, Compos. Struct., 93 (2011) 2083–2089.

[9] L.L. Ke, Y.S. Wang, Z.D. Wang, Nonlinear vibration of the piezoelectric nanobeams based on the nonlocal theory, Compos Struct., 94 (2012) 2038–2047.

[10] C. Liu, L.L. Ke, Y.S. Wang, J. Yang, Kitipornchai S. Buckling and post-buckling of size-dependent piezoelectric Timoshenko nanobeams subject to thermo-electro-mechanical loadings, Int. J. Struct. Stab. Dy., 14 (2014) 1350067.

[11] T. Murmu, J. Sienz, S. Adhikari, C. Arnold, Nonlocal buckling of double-nanoplate-systems under biaxial compression, Composites: Part B, 44 (2013) 84–94.

[12] P. Malekzadeh, A. Alibeygi, Thermal Buckling Analysis of Orthotropic Nanoplates on Nonlinear Elastic Foundation, Encyclopedia of Thermal Stresses., (2014) 4862-4872.

[13] M. Mohammadi, A. Farajpour, A. Moradi, M. Ghayour, Shear buckling of orthotropic rectangular graphene sheet embedded in an elastic medium in thermal environment, Composites: Part B, 56 (2014) 629–637.

[14] N. Radic, D. Jeremic, S. Trifkovic, M. Milutinovic, Buckling analysis of double-orthotropic nanoplates embedded in Pasternak elastic medium using nonlocal elasticity theory, Composites: Part B, 61 (2014) 162–171.

[15] D. Karlicic, S. Adhikari, T. Murmu, Exact closed-form solution for non-local vibration and biaxial buckling of bonded multi-nanoplate system, Composites: Part B, 66 (2014) 328-339.

[16] A. Anjomshoa, A.R. Shahidi, B. Hassani, E. Jomehzadeh, Finite Element Buckling Analysis of Multi-Layered Graphene Sheets on Elastic Substrate Based on Nonlocal Elasticity Theory, App. Math. Model., 38 (2014) 1-22.

[17] I.S. Radebe, S. Adali, Buckling and sensitivity analysis of nonlocal orthotropic nanoplates with uncertain material properties, Composites: Part B, 56 (2014) 840–846.

[18] L.Y. Jiang, Z. Yan, Vibration and buckling analysis of a piezoelectric nanoplate considering surface effects and in-plane constraints, Proc. R. Soc. A., 468 (2012) 3458-3475.

[19] M.E. Golmakani, J. Rezatalab, Nonuniform biaxial buckling of orthotropic Nano plates embedded in an elastic medium based on nonlocal Mindlin plate theory, Compos. Struct., 119 (2015) 238-250.

[20] N. Challamel, F. Hache, I. Elishakoff, C.M. Wang, Buckling and vibrations of micro structured rectangular plates considering phenomenological and lattice-based nonlocal continuum models, Compos. Struct., 149 (2016) 145-156.

[21] N. Radic, D. Jeremić, Thermal buckling of double-layered graphene sheets embedded in an elastic medium with various boundary conditions using a nonlocal new first-order shear deformation theory, Composites: Part B, 97 (2016) 201–215.

[22] M. Malikan, M. Jabbarzadeh, Sh. Dastjerdi, Non-linear Static stability of bi-layer carbon nanosheets resting on an elastic matrix under various types of in-plane shearing loads in thermo-elasticity using nonlocal continuum, Microsyst. Technol., 23 (2017) 2973-2991.

[23] Xue-Qian Fang, Chang-Song Zhu, Size-dependent nonlinear vibration of nonhomogeneous shell embedded with a piezoelectric layer based on surface/interface theory. Compos. Struct., 160 (2017) 1191–1197.

[24] Chang-Song Zhu, Xue-Qian Fang, Jin-Xi Liu, Hai-Yan Li., Surface energy effect on nonlinear free vibration behavior of orthotropic piezoelectric cylindrical nano-shells. Euro. J. of Mech. A/Solids, 66 (2017) 423-432.

[25] R.D. Mindlin, Influence of Rotatory Inertia and Shear on Flexural Motions of Isotropic, Elastic Plates. Trans. ASME, 73 (1951) 31–38.

[26] H.T. Thai, D.H. Choi, A simple first-order shear deformation theory for laminated composite plates, Compos. Struct., 106 (2013) 754–763.

[27] R.D. Mindlin, H.F. Tiersten, Effects of couple-stresses in linear elasticity, Arch Ration Mech Anal, 11 (1962) 415–48.

[28] R.A. Toupin, Elastic materials with couple stresses, Arch Ration Mech Anal, 11 (1962) 385–414.

[29] W.T. Koiter, Couple stresses in the theory of elasticity, I and II. Proc K Ned Akad Wet (B), 67 (1964) 17–44.

[30] E. Cosserat, F. Cosserat, Theory of deformable bodies. In: Delphenich DH, editor. Scientific Library, 6. Paris: A. Herman and Sons, Sorbonne 6; 1909.

[31] F. Yang, A.C.M. Chong, D.C.C. Lam, P. Tong, Couple stress based strain gradient theory for elasticity, Int. J Solids Struct, 39 (2002) 2731–43.

[32] B. Akgöz, Ö. Civalek, Free vibration analysis for single-layered graphene sheets in an elastic matrix via modified couple stress theory, Materials and Design., 42 (2012) 164–171.

[33] H.T. Thai, P.V. Thuc, T.K. Nguyen, Jaehong Lee, Size-dependent behavior of functionally graded sandwich microbeams based on the modified couple stress theory, Compos. Struct., 123 (2015) 337–349.

[34] C. Liu, L.L. Ke, J. Yang, S. Kitipornchai, Y.S. Wang, Buckling and post-buckling analysis of size-dependent piezoelectric nanoplates, Theo. & Appl. Mech. Lett., 6 (2016) 253-267.

[35] L.L. Ke, C. Liu, Y.S. Wang, Free vibration of nonlocal piezoelectric nanoplates under various boundary conditions, Physica E 66 (2015) 93–106.

[36] Q. Wang, Axi-symmetric wave propagation in a cylinder coated with a piezoelectric layer, Int. J. Solid Struct., 39 (2002) 3023–3037.

[37] M. Malikan, Electro-mechanical shear buckling of piezoelectric nanoplate using modified couple stress theory based on simplified first order shear deformation theory, Appl. Math. Model., 48 (2017) 196–207.

[38] M. Malikan, (2017). Analytical predictions for the buckling of a nanoplate subjected to nonuniform compression based on the four-variable plate theory, J. of Appl. and Comput. Mech., 3 (2017) 218–228.

[39] M. Malikan, (2017). Buckling analysis of a micro composite plate with nano coating based on the modified couple stress theory, J. of Appl. and Comput. Mech., 4 (2018) 1–15.

[40] M.E. Golmakani, M.N. Sadraee Far, Buckling analysis of biaxially compressed double-layered graphene sheets with various boundary conditions based on nonlocal elasticity theory, Microsyst. Technol., 23 (2017) 2145-2161.

[41] R. Ansari, S. Sahmani, Prediction of biaxial buckling behavior of single-layered graphene sheets based on nonlocal plate models and molecular dynamics simulations, Appl. Math. Modell., 37 (2013) 7338–51.